PAPER

Check for updates

Unravelling the influence of side-chain symmetry on device performance: insights from isoindigo-based polymers in thin-film transistors†

Anita Hu,[a] Audithya Nyayachavadi,[a] Max Weires,[b] Garima Garg,[a] Sihong Wang[b] and Simon Rondeau-Gagné*[a]

Thin-film transistors are at the basis of next-generation electronics and bioelectronics, with functionality beyond that of traditional silicon-based devices. To move forward with emerging soft and human-integrated technologies, innovations not only in molecular design, but also in device engineering, are required to access improved performance, stability, and biocompatibility. In this study, π-conjugated isoindigo–bithiophene donor–acceptor polymers were designed and synthesized to possess different side-chain symmetries. Polymers possessing symmetric branched alkyl side chains, symmetric oligoethylene glycol side chains, or asymmetric side chains were synthesized, and their properties were evaluated in two types of thin-film transistors to examine the influence of side-chain design on key materials properties. The results from a multimodal characterization showed that the design of semiconducting polymers with asymmetric side chains can lead to materials with balanced optoelectronic and solid-state properties. The polymer designs exhibited differing levels of performance when implemented in each of the two types of fabricated transistors The properties of the polymer, including crystallinity, thin-film morphology, and swelling, impacted the material's performance in the organic field-effect and electrochemical transistors. While the asymmetric design was beneficial for charge transport in field-effect transistors, a highly polar and symmetric polymer, beyond the amphiphilicity of the asymmetric species, led to improved device characteristics in electrochemical transistors. Overall, this study uncovered insightful trends in the structures and device performance of conjugated polymers with different side-chain symmetries, thus informing new design strategies for a future of efficient, long-lasting biocompatible devices.

Introduction

Electronic devices are constantly evolving in today's modern age, with demands pushing for faster conductivity, rapid information processing, and enhanced biocompatibility that can revolutionize the human user experience.[1–3] Developing organic electronics is key to ushering in this new generation of technology. Charge transport through these devices is enabled

[a]*Department of Chemistry and Biochemistry, University of Windsor, 401 Sunset Avenue, Windsor, Ontario N9B 3P4, Canada. E-mail: srondeau@uwindsor.ca*
[b]*Pritzker School of Molecular Engineering, University of Chicago, Chicago, Illinois 60637, USA*

†Electronic supplementary information (ESI) available: Experimental procedures, synthetic procedures for all monomers and polymers, ^{1}H-NMR, ^{13}C-NMR, and DOSY spectra, FTIR spectroscopic data, UV-vis absorption spectroscopic data, cyclic voltammetry, thermogravimetric analysis, OFET mobility equation, OFET output curve, OECT figure of merit equations, OECT transfer, transconductance, output, and cycling stability curves. See DOI: https://doi.org/10.1039/d3lp00104k

by a thin film of a fine-tunable organic semiconductor.[4] Organic thin-film electronics come in various design architectures, each promoting charge transport through the device by different means, such as electric field effects, ion conduction and doping, or other physicochemical means.[5] So far, organic electronic devices have achieved a range of practical functionalities and applications, including skin-like flexibility,[6] high-efficiency power generation,[7] health diagnostics, and more.[8,9]

π-Conjugated semiconducting polymers, a class of organic materials, are an exciting and emerging platform to develop flexible and conformable electronic devices. These materials have electronic properties comparable to those of amorphous silicon and can be tailored by chemical design for various technological applications, even rendered stretchable for wearable and on-skin electronics.[3,4,6] New designs and applications of semiconducting polymers in organic electronics have emerged in recent years, but these materials often have poor solubility in common organic solvents due to their extensive π-conjugation and strong aggregation properties.[10] In order to

process these materials in solution for large-area electronics *via* solution printing, the polymers are typically designed with long alkyl chains that can improve solubility in common organic chlorinated solvents.[11] These side chains are not only critical for processability, but their design is key for various important material properties, including solid-state packing, π–π stacking distance, and backbone rigidity/planarity that affects the polymer film crystallinity.[12,13] Throughout the years, many side-chain engineering strategies have been reported to access high-performance materials, stretchable polymers, and other innovative materials, utilizing components such as siloxane side chains, moieties enabling non-covalent interactions, and other designs.[14–16]

Among the various strategies that have been developed for tuning the solid-state structure and packing of conjugated polymers for electronic performance, asymmetric side-chain engineering, defined as functionalizing the semiconducting polymer with two different side-chain motifs, has become an emerging approach to modulate the thermomechanical, opto-electronic, and solid-state properties of these materials in organic electronics.[14,17–24] Particularly, the combination of solubilizing branched alkyl chains in combination with carbosilane chains has been shown to improve the charge carrier mobility, power conversion efficiency (PCE), and stability of materials in thin-film transistors and photovoltaic devices.[14,21,24] Notably, Lin *et al.* reported a systematic study of a library of asymmetric side chain isoindigo-based polymers using different types of carbosilane groups.[14] The authors discovered that careful selection of side chain combinations leads to both enhanced mechanical properties as well as hole mobilities (μ_h) as high as 3.49 cm^2 V^{-1} s^{-1} in organic field-effect transistors (OFETs). The design of materials with asymmetric side chains has also been applied to other semiconducting materials, including diketopyrrolopyrrole and naphthalene diimide-based materials.[20–24]

While still an emerging approach, thus far, most reported asymmetric side-chain engineering designs have focused on side-chain combinations with nonpolar motifs, with few studies investigating the combination of side chains with different properties (*i.e.*, chirality, polarity, functionalization, *etc.*).[21,23,24] In this context, asymmetric side-chain engineering to develop amphiphilic-type conjugated polymers remains a relatively new approach and one that carries a lot of potential for modulating structure–electronic property relationships of organic electronics. Previous reports have investigated symmetric, ambipolar polymers with hybrid side chains that combined both polar and non-polar moieties in one chain.[25,26] Although these hybrid polymers exhibited improved charge transport and device operational stability, asymmetric polymers with completely different side chains on either end of the monomer residues should further modulate solid-state packing and film crystallinity.[14,17,20] Previous reports on the amphiphilic functionalization of small-molecule organic semiconductors also confirmed that the asymmetric design can potentially improve self-assembly, increase solid-state order, and improve processing and electronic performance in devices.[27]

Recently, our group reported the development of an amphiphilic-designed asymmetric isoindigo–bithiophene (iI–BT) polymer with one solubilizing branched alkyl chain and one terminal dodecanol side chain, towards understanding the influence of an asymmetric polar head group on the electronic and processing capabilities of conjugated polymers.[19] In our findings, we discovered that through the incorporation of a simple terminal hydroxyl group per monomer residue, the solubility of the material was able to be altered, becoming processable in greener, non-chlorinated solvents, and achieving higher hole charge carrier mobility when used in OFETs. Notably, when investigated using cryogenic electron microscopy (Cryo-EM), it was found that the polymer exhibited long-range, fiber-like aggregation, suggesting that in addition to the asymmetric nature, the amphiphilic design could promote ordered self-assembly. Furthermore, the terminal hydroxyl group was shown to be susceptible to post-functionalization, demonstrating that amphiphilic side-chain engineering is a versatile and multifaceted approach for developing novel materials with enhanced properties. Another notable investigation on amphiphilic, asymmetric side-chain engineering was conducted by Yang *et al.*, in which diketopyrrolopyrrole-based polymers of different side chain symmetries were synthesized and tested in thin-film transistors.[20] The authors found that the asymmetric polymer with a triethylene glycol side chain and a branched alkyl side chain demonstrated more ordered self-assembly in thin film and higher hole mobility than both the symmetric polymer of only alkyl side chains and the copolymer with symmetric alkyl or ethylene glycol side chains per monomer residue. These findings implicate the unique microstructural and electronic properties that can be elucidated by an asymmetric polymer design, especially one containing side chains of different polarities.

To better understand the implications of amphiphilic asymmetric side-chain engineering in conjugated polymers and to compare symmetric *versus* asymmetric side-chain designs in different electronic devices, herein, we report the synthesis and characterization of iI–BT conjugated polymers that incorporate polar oligo(ethylene glycol) (EG) side chains in combination with a solubilizing branched alkyl side chain. A careful investigation of the influence of amphiphilicity on structure–property relationships in both OFETs and organic electrochemical transistors (OECTs) was performed, as illustrated in Fig. 1. To investigate the influence of asymmetry on polymer properties and in organic electronics, a symmetric hydrophobic polymer with only branched alkyl side chains (**P1**) and a symmetric hydrophilic polymer with only EG side chains (**P2**) were designed to test against the asymmetric polymer (**P3**), which contained one EG side chain and one branched alkyl side chain per monomer residue. Ethylene glycol (EG) side chains are a topic of great interest in the field of organic electronics because they are able to promote the self-assembly of conjugated molecules through phase segregation, alter the solubility of materials, and provide improved mechanical properties (due to the flexibility afforded by oxygen atoms) and conduction (due to their polar nature).[20,28–30] For these

© 2023 The Author(s). Published by the Royal Society of Chemistry

RSC Appl. Polym., 2023, **1**, 292–303 | **293**

Fig. 1 Poly(isoindigo-*co*-bithiophene) (P(iI–BT)) polymers of varying side-chain symmetries as semiconducting layer in OFET and OECT devices.

reasons, a hexyl EG side chain was selected to explore the impact of symmetric *versus* asymmetric side-chain designs in semiconducting polymers. Notably, this side chain has been successfully employed in polythiophene-based polymers, leading to organic electrochemical transistors with excellent characteristics.[31] Additionally, a 4-decyltetradecyl side chain was employed as the alkyl chain since it has been shown to lead to semiconducting polymers with high crystallinity and high charge carrier mobility.[18,32] Upon characterization of optoelectronic properties using UV-vis spectroscopy and cyclic voltammetry, the materials were then spin-coated into thin films to study their morphologies. When investigated through grazing-incidence wide-angle X-ray scattering (GIWAXS) and atomic force microscopy (AFM), the asymmetric polymer, **P3**, exhibited the longest-range order and improved thin-film crystallinity, which was reflected in its performance when integrated in OFETs displaying charge carrier mobility two orders of magnitude higher than both **P1** and **P2**. In OECTs, the EG-containing polymer **P2** demonstrated the highest performance and best device characteristics, confirming that symmetric EG side chains can give sufficient swellability for aqueous electrolytes to allow ion conduction and bulk doping in OECTs. Despite this finding, when integrated into OECTs, **P3** demonstrated greater cycling stability on select substrates that was attributed to its amphiphilic nature balancing polymer adhesion to the nonpolar substrate and ion interaction with

the hydrophilic electrolyte solution. Overall, this work confirms that side-chain design is key to achieving good device characteristics and performance and providing new avenues for materials optimization through either symmetric or asymmetric designs in both OFETs and OECTs.

Results and discussion

Synthesis and general characterization

Three different isoindigo–bithiophene (iI–BT) polymers were synthesized by slightly modified procedures from previous literature, as detailed in ESI (Schemes S1–S4†).[19,26,32–35] The synthesis of the three different monomers was performed *via* alkylation of isoindigo with the selected side-chain halides or tosylates under basic conditions. The symmetric monomers, **M1** and **M2**, only required the addition of one side chain each: hydrophobic compound **1** for **M1** and hydrophilic compound **2** for **M2**. To afford asymmetric monomer **M3**, equimolar amounts of compound **1** and compound **3** were added to the reaction vessel simultaneously to perform the alkylation in one pot. For each alkylation, the crude product mixture was purified by column chromatography to isolate the monomer of interest. The symmetric monomers, **M1** and **M2**, were afforded in moderate yields (43% and 45%, respectively). However, due to the various side reactions occurring within the one-pot

alkylation for **M3**, the yield of the asymmetric monomer was lower (20%). After chromatography, all three monomers were characterized by [1]H- and ^{13}C-nuclear magnetic resonance (NMR) spectroscopy and mass spectroscopy, as shown in ESI.† Monomers **M1** to **M3** were then polymerized with 5,5′-bis(trimethylstannyl)-2,2′-bithiophene *via* Stille cross-coupling to produce three different polymers: symmetric hydrophobic polymer **P1**, symmetric hydrophilic polymer **P2**, and asymmetric amphiphilic polymer **P3** (Scheme S4†). Each polymer was purified by successive Soxhlet extractions, followed by precipitation in methanol and drying under vacuum. All three polymers were then characterized by variable temperature ^{1}H-NMR spectroscopy at 120 °C in 1,1,2,2-tetrachloroethane-d_2. Furthermore, to characterize the different functional groups of each polymer, Fourier-transform infrared (FTIR) spectroscopy was conducted on the polymers in the solid state (Fig. S1†). Notably, at 1200 cm^{-1} in the FTIR spectra, the C–O stretching peak gradually increased in intensity as the hydrophilicity of the polymers—represented by the ethylene glycol (EG) content in the side chains—increased. Also, the C–H stretching around 2700 cm^{-1}, C=O stretching around 1700 cm^{-1}, and C=C stretching around 1650 cm^{-1} all increased in intensity with increasing hydrophilicity. Changes in C–H bond polarity were also seen in the NMR spectra of the three monomers and polymers, where the chemical shifts of the protons and carbon atoms of the EG side chains were more downfield than those of the alkyl side chains.

Following structural characterization, further chemical and optical characterizations were conducted on the three polymers, and the results are summarized in Table 1. Firstly, high-temperature gel-permeation chromatography (GPC) was used to evaluate the molecular weights of the polymers, **P1** and **P3**, which were found to be 27.0 and 22.9 kDa, respectively. Surprisingly, the molecular weight determination by GPC for **P2** was unsuccessful, as the calculated M_n of **P2** from GPC (0.6 kDa) was less than the molecular weight of the monomer **M2** (976 g mol^{-1}). This was attributed to limited solubility of the hydrophilic polymer, **P2**, in 1,2,4-trichlorobenzene, the solvent used for GPC. Thus, an alternative procedure was per-

formed to attempt to measure the molecular weight (M) of the three polymers *via* diffusion-order NMR spectroscopy (DOSY).[36] The diffusion coefficients of polystyrene standards were determined experimentally by DOSY, then plotted logarithmically against the log of the standards' known molecular weights. After experimentally determining the diffusion coefficient (D) of **P2**, the polymer's molecular weight was then estimated from the log(D) *vs.* log(M) line of best fit to be 15.6 kDa. Unfortunately, we encountered challenges in obtaining DOSY measurements for **P1** due to its significantly low solubility in chloroform at room temperature. However, in contrast, the asymmetric polymer **P3** exhibited much better solubility in CDCl$_3$ at room temperature, enabling us to use DOSY for accurate molecular weight determination. As a result, a molecular weight of 15.8 kDa was measured for **P3**, consistent with the value obtained through GPC (22.9 kDa). Notably, DOSY also showed a higher diffusion peak for **P3**, estimated to a molecular weight of 86.1 kDa,. Due to the varying procedures for molecular weight determination, the degree of polymerization for all three polymers was calculated, yielding relatively similar values as reported in Table 1.

Next, UV-visible (UV-vis) spectroscopy was conducted to assess the optical properties of the polymers in both the solution and solid states (Fig. S2†). In both states, **P1** had the shortest wavelength of maximum absorbance (691 nm), while **P2** had the longest (722 nm) and was thus the most redshifted. Although the asymmetric **P3** had maximum absorbance at a wavelength between both symmetric polymers (717 nm), its wavelength was much closer in value to the hydrophilic polymer, **P2**. The longer absorption wavelengths of **P2** and **P3** compared to **P1** may suggest that the hydrophilic EG side chains promote increased effective conjugation within the polymer material. Previous reports have found that polymer films containing linear polar moieties demonstrated significant red-shifting due to their crystalline chain packing because of the polar bonds' dipole–dipole interactions and linear chains enabling closer π–π stacking.[29,37] Similarly, the oxygen-containing EG side chains may promote high polymer crystallinity, leading to enhanced effective conjugation of the

Table 1 Molecular weights, polydispersity indices, optoelectronic properties, and decomposition temperatures of semiconducting polymers **P1** to **P3**

	$M_n{}^a$ (kDa)	$M_w{}^a$ (kDa)	M^b (kDa)	$Đ_w{}^c$	DP^d	$\lambda_{max, solution}{}^e$ (nm)	$\lambda_{max, film}{}^f$ (nm)	$E_g^{opt\ g}$ (eV)	$E_{HOMO}{}^h$ (eV)	$E_{LUMO}{}^i$ (eV)	$T_d{}^j$ (°C)
P1	27.0	141.6	—^{l}	5.3	21	691.3	704.2	1.46	−5.16	−3.70	337
P2	0.6^k	3.9^k	15.6	6.5	14	722.4	735.0	1.55	−5.05	−3.50	336
P3	22.9	90.1	15.8, 86.1	3.9	19	717.0	730.9	1.50	−5.09	−3.59	369

^{a} Number-average molecular weight and weight-average molecular weight estimated by high-temperature gel permeation chromatography (GPC) in 1,2,4-trichlorobenzene at 180 °C using polystyrene as standard. ^{b} Molecular weight estimated by diffusion-order NMR spectroscopy (DOSY) in CDCl$_3$ using polystyrene as standard (see ESI† for procedure). ^{c} Dispersity defined as M_w/M_n. ^{d} Degree of polymerization defined as M_n/M_0 for **P1** and **P3** or M/M_0 for **P2**, where M_0 is the molecular weight of the repeat unit of each polymer. ^{e} Absorption maxima in dilute solution of chloroform. ^{f} Absorption maxima in thin film. ^{g} Optical bandgap calculated by the following equation: $E_g^{opt} = 1240/\lambda_{max\ onset}$ of polymer film. ^{h} Calculated from cyclic voltammetry (potentials *vs.* Ag/AgCl) using 0.1 M TBAPF$_6$ in CH$_3$CN as electrolyte where $E_{HOMO} = -4.38$ eV − (Ox$_{onset}$). ^{i} Estimated from calculated E_g^{opt} and E_{HOMO}. ^{j} Estimated from thermogravimetric analysis (TGA) at 5% mass loss. ^{k} Due to insolubility of the hydrophilic polymer, **P2**, in 1,2,4-trichlorobenzene, molecular weight determination by GPC was unsuccessful; DOSY in CDCl$_3$ was alternatively used to estimate the molecular weight (M) of **P2** (see footnote b). ^{l} Due to low solubility of hydrophobic polymer, **P1**, in CDC1$_3$, molecular weight determination by DOSY was unsuccessful.

polymer backbones and the observed red shift in absorbance. Solid-state UV-vis spectroscopy and cyclic voltammetry (CV) were used to calculate the optical bandgap energy and highest occupied molecular orbital (HOMO) energy, respectively, of the three polymers (Fig. S2b and S3†). The lowest unoccupied molecular orbital (LUMO) energy was then calculated from the sum of the optical bandgap and HOMO energy. As summarized in Table 1, all three polymers demonstrated similar HOMO and LUMO energy levels characteristic of organic semiconducting polymers.[14,19,32] The decomposition temperatures of the polymers were measured by thermogravimetric analysis (Fig. S4†). All three polymers exhibited good thermal stability, within the range of other iI–BT polymers reported in literature.[18,32] **P1** and **P2** had similar decomposition temperatures at 5% weight loss, but **P3** required the highest temperature for weight decomposition by 5%, which may be the result of the asymmetric design.

To assess the film morphology of the polymer materials, grazing-incidence wide-angle X-ray scattering (GIWAXS) and atomic force microscopy (AFM) were conducted. Thin films were prepared by spin-coating a 5 mg mL^{-1} solution of each polymer in 1,1,2,2-tetrachloroethane on phenyltrimethoxysilane (PTS)-treated Si/SiO$_2$ wafers.[38] Fig. 2 shows the 2D plots of X-ray scattering and the AFM height and phase images of each polymer, and Table 2 reports the three polymer films' root-mean-square surface roughness values, as well as the calculated π–π stacking and lamellar spacing distances from the 1D plots of q_{xy} and q_z, respectively. The findings illustrated relatively amorphous and smooth films among all polymers. Based on the out-of-plane q_{xy} reflections, the π–π stacking distances of all three polymer films were consistent. On the other hand, from the in-plane q_z reflections, lamellar spacing varied among the films. **P1** did not exhibit any significant lamellar stacking, whereas **P2** and **P3** exhibited relatively similar amounts, suggesting that the presence of EG side chains may promote higher film crystallinity—a trend that would be consistent with our optoelectronic analyses where **P2** and **P3** exhibited the most effective conjugation. This can be attributed to the hydrophilicity of the EG side chains, combined to their linear structure that can promote better self-assembly in the solid-state. Furthermore, assessing the full width at half maximum (FWHM) for the in-plane lamellar spacing peaks, **P3** had a lower value than **P2**, indicating that the crystallite size of **P3** was larger and should thus promote higher order in the film. Therefore, from the GIWAXS findings, the asymmetric polymer design seemed to promote higher polymer chain order in the solid state. Based on the AFM data, surface roughness was found to be highest in **P2**, further illuminating a trend between increasing EG content and greater, rougher crystalline packing (Fig. 2). From the AFM height and phase images in Fig. 2, **P1** exhibited the most fiber-like morphology, and **P2** exhibited the most film aggregation out of the three polymers, which would support the findings from GIWAXS of **P2**'s relatively large crystallite domains (Fig. 2b). Finally, **P3** exhibited relatively aligned polymer fibre morphology over a long range, as seen in its phase image in Fig. 2c. The aligned

fibres of **P3** thus demonstrate the polymer's intermediate properties between the highly fibrous **P1** and aggregated **P2**.

Asymmetric *versus* symmetric side-chain engineering in organic field-effect transistors (OFETs)

Upon characterization of the optoelectronic and solid-state properties of the three semiconducting polymers, organic field-effect transistors (OFETs) were fabricated using each polymer to compare their charge transport properties and compare the two side-chain designs. The experimental procedure for the fabrication of the bottom-gate top-contact OFET devices is detailed in ESI.† Briefly, a solution of each polymer was prepared in 1,1,2,2-tetrachloroethane (5 mg mL^{-1}) then spun-coat onto phenyltrimethoxysilane (PTS)-treated Si/SiO$_2$ wafers at 1000 rpm.[39] Notably, a phenyltrimethoxysilane (PTS) monolayer was used as a surface functionalization strategy to improve film quality and wettability.

Fig. 3 shows the transfer and output curves of the three polymers, and Table 3 summarizes the measurements of each polymer film's average device performance. The hole mobilities and average threshold voltage values were calculated in the forward sweep direction for all OFET devices. The equation used to calculate hole mobilities is reported in ESI.† Observing the output curves, all three polymers' devices demonstrated behaviour that was characteristic of an OFET in accumulation mode: drain current (I_D) became more strongly negative as the source–drain voltage (V_D) strengthened in magnitude with each additional −20 V bias of the gate voltage. However, non-ideal saturation behaviour was seen by all polymers at low V_D (between 0 and −10 V), where positive I_D values were measured (Fig. 3). As discussed in previous reports, this phenomenon may be the result of charge injection from the gold source electrode into the polymer channel, thus building up some contact resistance at low V_D and leading to initially reversed current.[19,40] To better contrast the performances of the three different polymers, Fig. S5† illustrates the output curves of the three polymers along the same scale range of I_D (from −3.0 × 10^{-7} to 5.0 × 10^{-8} A). Notably, **P3** produced the strongest source–drain current responses, while **P1** demonstrated the weakest performance of the three polymers. The charge carrier mobilities of the devices were extracted from transfer curves that had V_D bias of −100 V, which lies within the saturation region of the output curves. Comparing the device performance values, **P3** showed the highest mobility (0.024 cm^2 V^{-1} s^{-1}) and greatest I_{on}/I_{off} current ratio (10^4)—one and two orders of magnitude higher than **P2** and **P1**, respectively (Table 3). This may be attributed to the long-range crystalline arrangement of the **P3** polymer film, as observed from GIWAXS. **P2** showed the second highest mobility (0.0048 cm^2 V^{-1} s^{-1}), while also having the second-most long-range ordered crystalline polymer alignment based on the GIWAXS data. Interestingly, **P1**, possessing symmetric alkyl chains, showed a relatively low charge mobility of 0.0004 cm^2 V^{-1} s^{-1} and I_{on}/I_{off} current ratio (10^2). Notably, while previous reports on **P1** and similar isoindigo-based copolymers have shown good charge transport behaviors on OTS-functionalized sub-
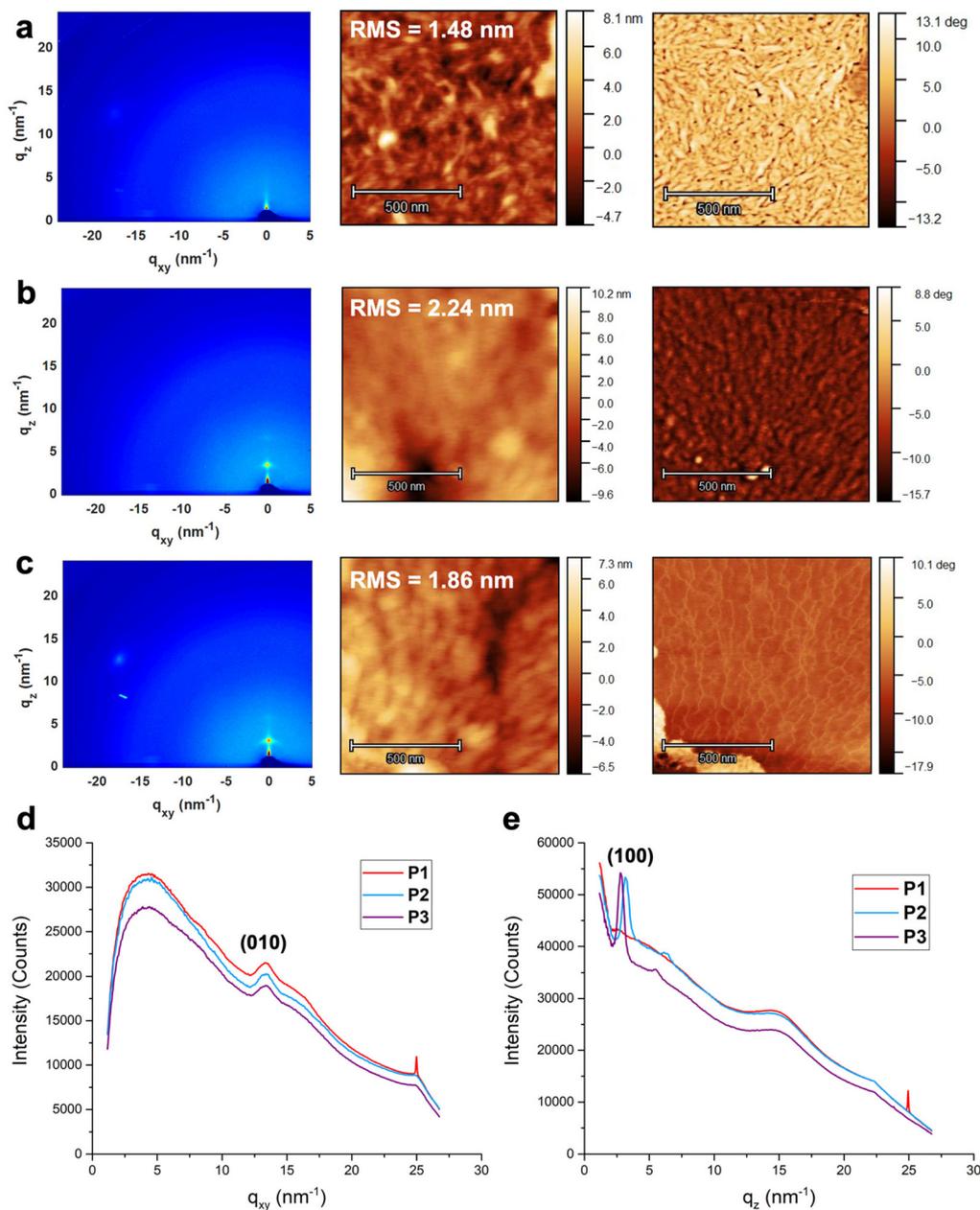
296 | *RSC Appl. Polym.*, 2023, **1**, 292–303

© 2023 The Author(s). Published by the Royal Society of Chemistry

Fig. 2 GIWAXS, AFM height, and AFM phase images (left to right, respectively) of (a) **P1**, (b) **P2**, and (c) **P3**. 1D profiles of (d) out-of-plane q_{xy} (010) reflections for all three polymers and (e) in-plane q_z (100) reflections for all three polymers. AFM scale bar is 500 nm.

Table 2 Root-mean-square film surface roughness (R_q), crystallographic d-spacing distances, and FWHM values for all three polymer films

| Film | R_q^{avg} (nm) | (010) π–π stacking | | (100) Lamellar stacking | |
		d (Å)	FWHM (Å^{-1})	d (Å)	FWHM (Å^{-1})
P1	1.78 ± 0.33	4.70	0.11	N/A	N/A
P2	2.61 ± 0.63	4.70	0.11	19.65	0.058
P3	1.66 ± 0.36	4.69	0.10	22.38	0.049

strate, the lack of lamellar order in **P1** on PTS may have contributed to the suboptimal performance in the current device architecture.[18,41] The difference between the two different surface-modified substrates has also been previously observed in the literature.[42] Overall, although all three polymers demonstrated characteristics of OFET performance, **P3**, bearing both alkyl and EG side chains, showed the best device characteristics. This result confirms that polymer designs with asymmetric side chains of different polarities can be an efficient method to structurally optimize semiconducting polymers in OFETs.

© 2023 The Author(s). Published by the Royal Society of Chemistry

RSC Appl. Polym., 2023, **1**, 292–303 | **297**
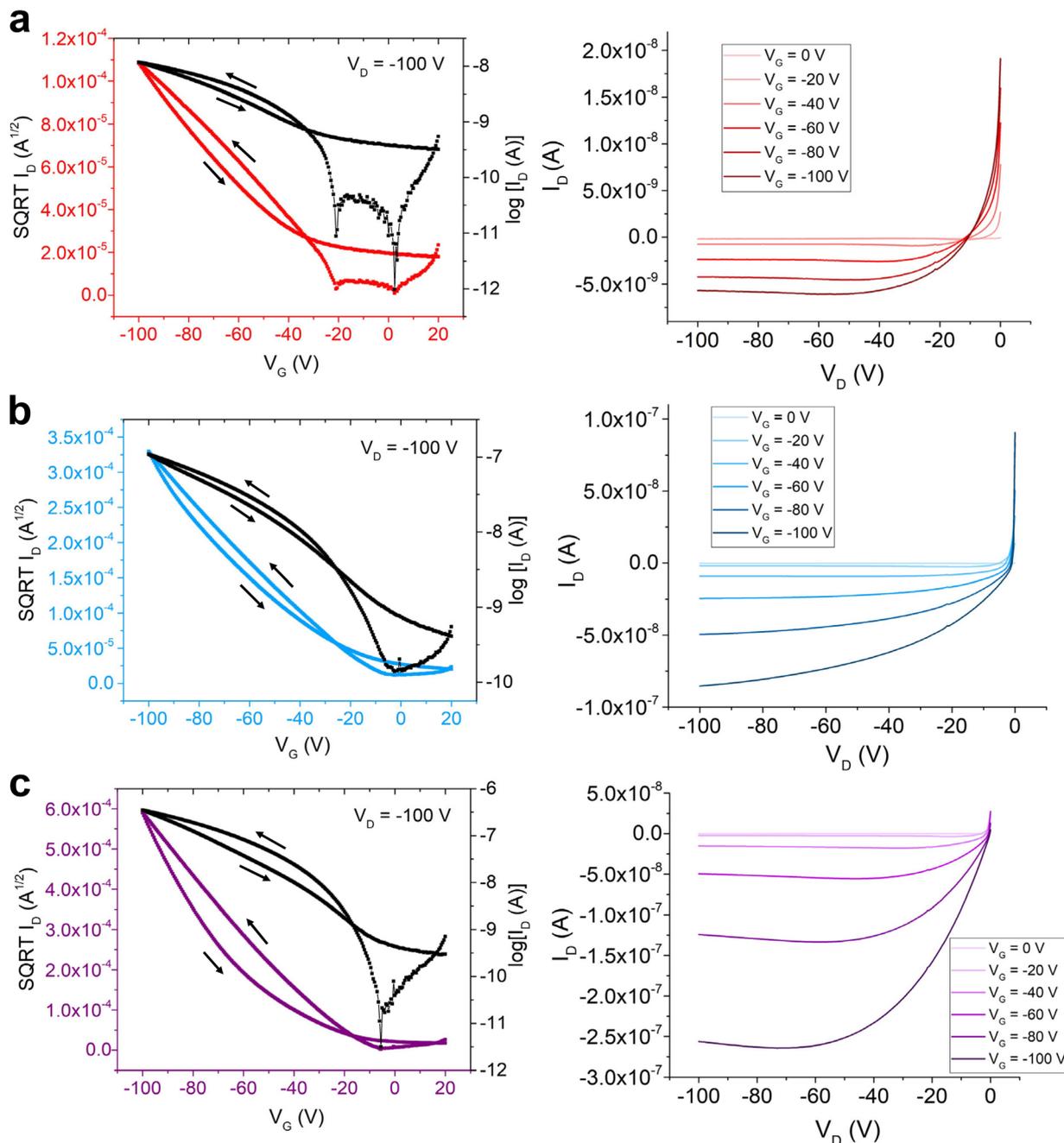
Fig. 3 OFET transfer curves (left) and output curves (right) of (a) **P1**, (b) **P2**, and (c) **P3**.

Table 3 Average and maximum hole mobilities (μ_h^{avg}, μ_h^{max}), I_{on}/I_{off} current ratios, and threshold voltages (V_{th}) for the OFETs. Results were averaged from 8 devices

Polymer	$\mu_h^{avg}\|\mu_h^{max}$ (cm^2 V^{-1} s^{-1})	$[I_{on}/I_{off}]^{avg}$	V_{th}^{avg} (V)
P1	$0.00040 \pm 0.00007\|0.00052$	10^2	-9.2
P2	$0.0048 \pm 0.0007\|0.0063$	10^3	-16.3
P3	$0.024 \pm 0.006\|0.034$	10^4	-27.4

Asymmetric *versus* symmetric side-chain engineering in organic electrochemical transistors (OECTs)

Among the emerging technologies investigated in organic electronics, organic electrochemical transistors (OECTs) are a promising device design for biocompatible electronics. OECTs operate on low voltages (<1 V), and their operation mechanism relies on the intercalation of ions into the semiconducting layer and resulting redox reaction of the polymer to transduce current through the device.[43,44] Since OECTs require ions from

the aqueous solution to penetrate the semiconducting layer and promote charge mobility, the conjugated polymer used in these devices must contain suitable moieties for ion inter-action, charge transport, and adhesion to an inert, often non-polar substrate.[45] Previous research has found that polymers containing both hydrophilic and hydrophobic components can maximize device performance and stability.[26] Thus, to test the stability of the three polymers, and to further compare the symmetric and asymmetric side-chain designs, OECTs were fabricated using **P1**, **P2**, and **P3**. The experimental procedure for the complete OECT device fabrication can be found in the ESI† under general procedure and materials. While OECTs can be fabricated on non-treated glass or SiO_2 substrates, this work explored OECT devices fabricated on (1) phenyltrimethoxysi-lane (PTS)-treated Si wafers, to compare OECT device perform-ance to the previous OFET and film morphology results that were all conducted on PTS-treated substrates, and (2) *n*-octade-cyltrimethoxysilane (OTS)-treated glass wafers. While charge carrier mobility was quantified for each OFET as a measure of device performance, two key figures of merit for OECTs are transconductance (g_m) and the product of the charge carrier mobility (μ) and volumetric charge storage capacitance (C^*).[46] Details regarding the calculations for g_m and μC^* values can be found in ESI.† The range of gate and source–drain voltages was selected based on the conventional low-voltage (<1 V) con-ditions for OECT operation and device biocompatibility.[44,47] Furthermore, the source–drain voltage bias for the transfer curves was selected to be relatively low (−0.1 V) in an attempt to optimize transconductance values at a relatively low gate voltage.[48]

Fig. 4 shows the transfer, transconductance, and output curves of the three polymers in OECTs, and Table 4 summar-izes the device measurements of each film's performance on PTS-treated substrates. The same curves for the polymer films on OTS-treated substrates can be found in Fig. S6,† with the measurements reported in Table S1.† The average threshold voltages were calculated in the forward sweep direction for all OECT devices. Analyzing the output curves in Fig. 4, only **P2** demonstrated performance characteristic of OECTs in accumulation mode. The drain current produced by **P2** in the OECT was significantly greater in magnitude than the drain currents produced by **P1** and **P3** in the OECTs. The transfer and transconductance curves of **P2** confirmed this material's performance and demonstrated that the ions that doped into the polymer to promote source–drain current during the device's accumulation stage reversibly returned to the aqueous solution and restored the device to an ion-depleted state, thus encouraging swelling and de-swelling of the polymer (Fig. 4b).[48] Possibly, the OECTs made from **P1** and **P3** may have begun to show characteristics of an output curve at stronger gate biases exceeding −0.8 V (Fig. 4a and c). However, the transfer and transconductance curves for **P1** and **P3** were very crudely representative of an OECT—only reach-ing very small negative current values and barely creating normal transconductance curves (Fig. 4a and c). Therefore, an average threshold voltage for the poor-performing **P1** was not

determined in the OECT devices, and the μC^* values for **P1** and **P3** were found to be negligible (Table 4). The results obtained from the characterization of OECTs on OTS-treated substrates were consistent with the findings on PTS-treated substrates. From the transfer and output curves in Fig. S6,† **P2** demonstrated the best device performance, whereas **P1** demonstrated the least characteristic performance of OECTs and **P3** demonstrated some device performance at higher drain voltage biases beyond −0.8 V. The maximum transcon-ductance and threshold voltage values of **P3** were also inter-mediate to those of **P1** and **P2** on the OTS-treated substrates, thus highlighting comparable results between the different monolayers. Despite the variation in OECT performance among the three polymers, the cycling of the OECT devices was assessed in the following tests to investigate the stability of the polymers in the OECTs over time. The devices were cycled on and off by repeatedly switching the gate voltage from 0.1 V (device should be off, $I_D = 0$ A) to −1.0 V (device should turn on, I_D = max). The switching curves of the three polymers' devices on PTS-treated substrate are individually plotted in Fig. S7.† Firstly, based on the graph scale, **P2** was the only significantly performing semiconducting layer in the OECT out of the three polymers tested, reaching drain cur-rents that were at least 2 orders of magnitude higher than **P1** and **P3**. **P2** demonstrated relatively stable performance upon repeated on–off switching, with the drain current slightly increasing in magnitude by 29% from the beginning to the end of testing. On the other hand, **P1** and **P3** demonstrated much less stability, increasing in drain current magnitude by 174% and 412%, respectively. Interestingly, the devices on OTS-treated substrate showed slightly different results, as illustrated in Fig. S8.† **P2** was shown to lose stability over time, as its current output decreased in magnitude by 48% (from -2.4×10^{-4} A to -1.25×10^{-4} A) after 160 s of oper-ation, stabilizing in performance around -1.25×10^{-4} A. Although **P1** and **P3** barely promoted drain current com-pared to **P2**, their cycled performances still showed interesting trends. **P1** increased in current output by 86% (from 7.0×10^{-8} A to 1.3×10^{-7} A) over 150 s of operation, possibly because of the build-up of ions doping the polymer and the nature of its branched alkyl side chains trapping some ions (Fig. S8a†). On the other hand, **P3** remained quite stable in performance over time, suggesting that this film may have been able to modulate ion doping and de-doping with each cycle and minimize film disturbance by the aqueous ions (Fig. S8c†). Interestingly, the findings on the OTS-treated sub-strates were similar to a previous report on OECT cycling stability, in which the most hydrophilic polymer of branched EG side chains displayed the most instability due to overoxi-dation and polymer swelling from its polar interactions with the ionic solution, whereas the polymer containing hybrid alkyl and ethylene glycol side chains demonstrated very high stability lasting 6 hours.[26] Therefore, although the hydrophilic polymer (**P2**) significantly outperformed the asymmetric polymer (**P3**) in terms of charge propagation through the OECT, the combined hydrophobic and hydrophilic com-
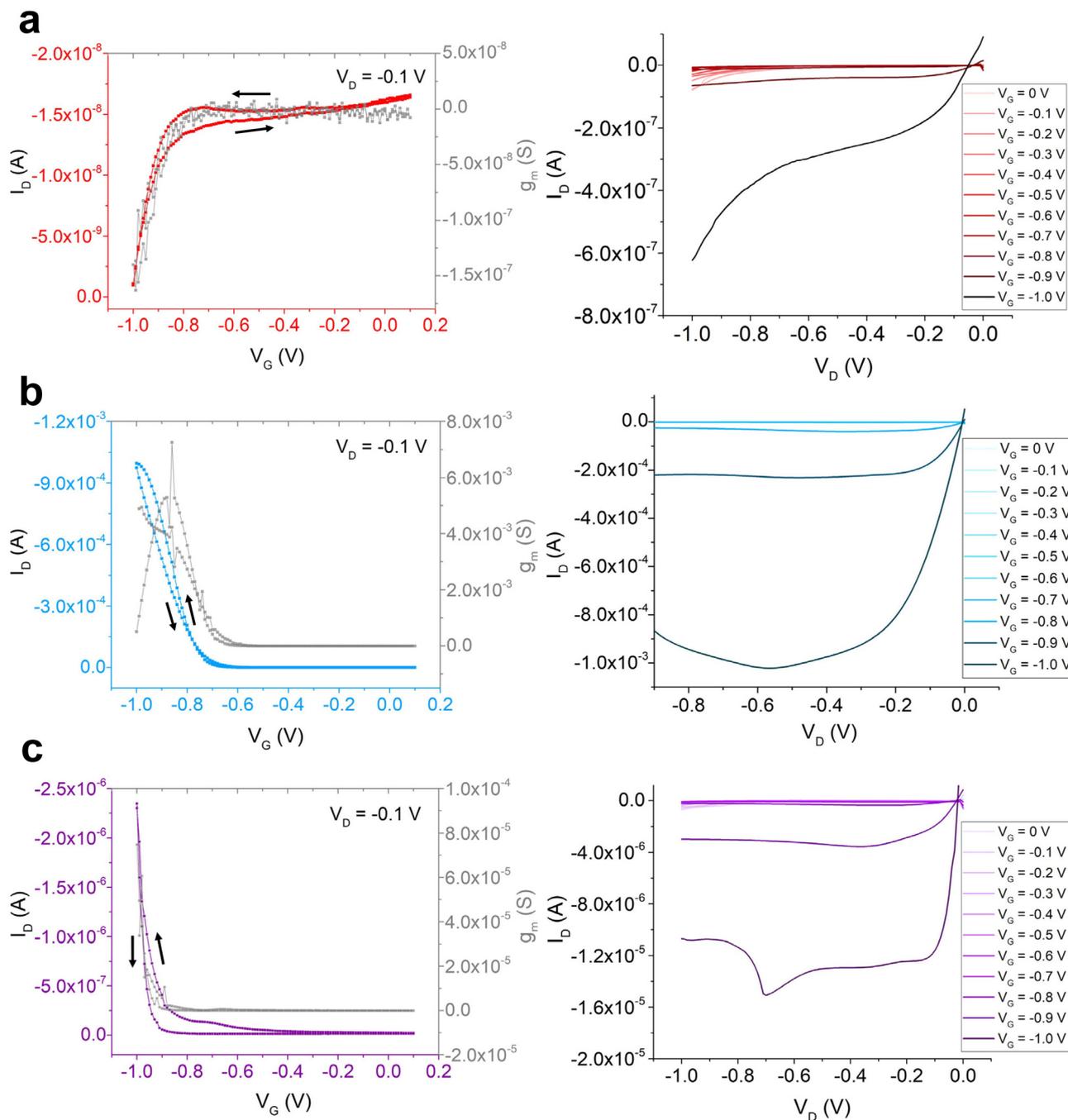
© 2023 The Author(s). Published by the Royal Society of Chemistry

RSC Appl. Polym., 2023, **1**, 292–303 | **299**

Fig. 4 OECT transfer and transconductance curves (left) and output curves (right) of (a) **P1**, (b) **P2**, and (c) **P3** on PTS-treated substrate.

Table 4 Maximum transconductances (g_m^{max}), I_{on}/I_{off} current ratios, threshold voltages (V_{th}), and μC^* for the OECTs on PTS-treated substrate

Film	g_m^{max} (S)	$[I_{on}/I_{off}]^{avg}$	V_{th}^{avg} (V)	μC^* (F cm^{-1} V^{-1} s^{-1})
P1	8.89×10^{-9}	10^1	N/A	N/A
P2	7.25×10^{-3}	10^3	-0.8	9.25×10^{-2}
P3	7.48×10^{-5}	10^2	-1.0	N/A

ponents of **P3** may still lead to greater operational stability, as elucidated by the asymmetric design, particularly on the OTS monolayer.

Conclusion

In conclusion, three different isoindigo-based polymers of varying side-chain symmetries and hydrophilicities were syn-

300 | *RSC Appl. Polym.*, 2023, **1**, 292–303

© 2023 The Author(s). Published by the Royal Society of Chemistry

thesized, characterized, and evaluated in thin-film transistors to compare and evaluate side-chain designs. NMR and FTIR spectroscopy confirmed the structures of all polymers, with the asymmetric species successfully being characterized with structural features between the two symmetric materials. The optoelectronic properties of all three polymers were similar in terms of the polymers' optical bandgaps and HOMO and LUMO energy levels, based on UV-vis spectroscopy and CV measurements, with the asymmetric species possessing values intermediate to the two symmetric polymers. Polymer film morphology was assessed by GIWAXS and AFM. All films were observed to be smooth, with film crystallinity increasing with greater EG content. The asymmetric **P3** demonstrated the longest-range order of the three polymers in thin film and a larger crystallite size than the symmetric, hydrophilic **P2**. These film morphologies helped to inform of the polymers' performances in OFETs, where **P3** demonstrated the highest average hole mobility, followed by **P2**, then **P1**. The results from the materials characterizations and OFET device testing indicated that asymmetric polymer design is a promising way to elucidate various material properties by balancing different side chains simultaneously. Informed of the trend that polymer asymmetry may benefit device performance in OFETs, the polymers were also tested in OECT devices to assess their potential as biocompatible organic semiconducting materials. **P2** successfully conducted current through the OECT at a low-magnitude threshold voltage (-0.8 V), demonstrating its promising potential as a semiconducting polymer for bio-applications. However, **P1** and **P3** were not hydrophilic enough to transduce significant current upon interacting with ions in solution. On–off cycling of the OECTs demonstrated varying results depending on the self-assembled monolayer, with **P3** exhibiting good stability on OTS-treated substrates and **P2** demonstrating stability on PTS-treated substrates. Nonetheless, the strong performance of **P2** indicates that the symmetric, hydrophilic polymer design prevailed as a candidate semiconducting material for OECT devices, relative to the asymmetric and more hydrophobic polymers tested in this investigation.

This work importantly contrasted the properties and performances of a set of symmetric and asymmetric semiconducting materials in two different types of thin-film transistors. On one hand, the asymmetric design balanced the optoelectronic and morphological properties afforded by either side chain, enhancing performance in OFETs. On the other hand, a symmetric design capitalized on certain properties, such as swelling and crystallinity, needed for successful performance specifically in OECTs. The properties and performances of the new materials investigated in this work highlight the need to further design materials of varying side chain symmetries and polarities that best perform for their application in emerging organic electronics.

Author contributions

All authors contributed to the manuscript. All authors have given approval to the final version of the manuscript.

Conflicts of interest

The authors declare no competing financial interest.

Acknowledgements

References

1 S. Holliday, J. E. Donaghey and I. McCulloch, Advances in charge carrier mobilities of semiconducting polymers used in organic transistors, *Chem. Mater.*, 2014, **26**, 647–663.

2 L. Shao, Y. Zhao and Y. Liu, Organic synaptic transistors: The evolutionary path from memory cells to the application of artificial neural networks, *Adv. Funct. Mater.*, 2021, **31**, 2101951.

3 M. L. Hammock, A. Chortos, B. C.-K. Tee, J. B.-H. Tok and Z. Bao, 25th anniversary article: The evolution of electronic skin (E-Skin): A brief history, design considerations, and recent progress, *Adv. Mater.*, 2013, **25**, 5997–6038.

4 X. Guo, M. Baumgarten and K. Müllen, Designing π-conjugated polymers for organic electronics, *Prog. Polym. Sci.*, 2013, **38**, 1832–1908.

5 M. Fahlman, S. Fabiano, V. Gueskine, D. Simon, M. Berggren and X. Crispin, Interfaces in organic electronics, *Nat. Rev. Mater.*, 2019, **4**, 627–650.

6 S. Dai, Y. Dai, Z. Zhao, F. Xia, Y. Li, Y. Liu, P. Cheng, J. Strzalka, S. Li, N. Li, Q. Su, S. Wai, W. Liu, C. Zhang, R. Zhao, J. J. Yang, R. Stevens, J. Xu, J. Huang and S. Wang, Intrinsically stretchable neuromorphic devices for on-body processing of health data with artificial intelligence, *Matter*, 2022, **5**, 3375–3390.

7 J. Fu, P. W. K. Fong, H. Liu, C. S. Huang, X. Lu, S. Lu, M. Abdelsamie, T. Kodalle, C. M. Sutter-Fella, Y. Yang and G. Li, 19.31% binary organic solar cell and low non-radiative recombination enabled by non-monotonic intermediate state transition, *Nat. Commun.*, 2023, **14**, 1760.

© 2023 The Author(s). Published by the Royal Society of Chemistry

RSC Appl. Polym., 2023, **1**, 292–303 | **301**

8 S. Casalini, F. Leonardi, T. Cramer and F. Biscarini, Organic field-effect transistor for label-free dopamine sensing, *Org. Electron.*, 2013, **14**, 156–163.

9 D. A. Bernards, D. J. Macaya, M. Nikolou, J. A. DeFranco, S. Takamatsu and G. G. Malliaras, Enzymatic sensing with organic electrochemical transistors, *J. Mater. Chem.*, 2008, **18**, 116–120.

10 T.-Q. Nguyen, R. Y. Yee and B. J. Schwartz, Solution processing of conjugated polymers: the effects of polymer solubility on the morphology and electronic properties of semiconducting polymer films, *J. Photochem. Photobiol., A*, 2001, **144**, 21–30.

11 J. Mei, Y. Diao, A. L. Appleton, L. Fang and Z. Bao, Integrated materials design of organic semiconductors for field-effect transistors, *J. Am. Chem. Soc.*, 2013, **135**, 6724–6746.

12 J. Y. Back, H. Yu, I. Song, I. Kang, H. Ahn, T. J. Shin, S.-K. Kwon, J. H. Oh and Y.-H. Kim, Investigation of structure-property relationships in diketopyrrolopyrrole-based polymer semiconductors via side-chain engineering, *Chem. Mater.*, 2015, **27**, 1732–1739.

13 J. Lee, J. W. Chung, J. Jang, D. H. Kim, J.-I. Park, E. Lee, B.-L. Lee, J.-Y. Kim, J. Y. Jung, J. S. Park, B. Koo, Y. W. Jin and D. H. Kim, Influence of alkyl side chain on the crystallinity and trap density of states in thiophene and thiazole semiconducting copolymer based inkjet-printed field-effect transistors, *Chem. Mater.*, 2013, **25**, 1927–1934.

14 Y.-C. Lin, F.-H. Chen, Y.-C. Chiang, C.-C. Chueh and W.-C. Chen, Asymmetric side-chain engineering of isoindigo-based polymers for improved stretchability and applications in field-effect transistors, *ACS Appl. Mater. Interfaces*, 2019, **11**, 34158–34170.

15 M. U. Ocheje, M. Selivanova, S. Zhang, T. H. V. Nguyen, B. P. Charron, C.-H. Chuang, Y.-H. Cheng, B. Billet, S. Noori, Y.-C. Chiu, X. Gu and S. Rondeau-Gagné, Influence of amide-containing side chains on the mechanical properties of diketopyrrolopyrrole-based polymers, *Polym. Chem.*, 2018, **9**, 5531–5542.

16 M. Mooney, Y. Wang, E. Iakovidis, X. Gu and S. Rondeau-Gagné, Carbohydrate-containing conjugated polymers: Solvent-resistant materials for greener organic electronics, *ACS Appl. Electron. Mater.*, 2022, **4**, 1381–1390.

17 H.-C. Yen, Y.-C. Lin and W.-C. Chen, Modulation of the hydrophilicity on asymmetric side chains of isoindigo-based polymers for improving carrier mobility-stretchability properties, *Macromolecules*, 2021, **54**, 1665–1676.

18 G. Xue, X. Zhao, G. Qu, T. Xu, A. Gumyusenge, Z. Zhang, Y. Zhao, Y. Diao, H. Li and J. Mei, Symmetry breaking in side chains leading to mixed orientations and improved charge transport in isoindigo-alt-bithiophene based polymer thin films, *ACS Appl. Mater. Interfaces*, 2017, **9**, 25426–25433.

19 M. Mooney, A. Nyayachavadi, A. Awada, E. Iakovidis, Y. Wang, M.-N. Chen, Y. Liu, J. Xu, Y.-C. Chiu, X. Gu and S. Rondeau-Gagné, Asymmetric side-chain engineering in semiconducting polymers: A platform for greener processing and post-functionalization of organic electronics, *Polym. Chem.*, 2023, **14**, 562–572.

20 S.-F. Yang, Z.-T. Liu, Z.-X. Cai, M. J. Dyson, N. Stingelin, W. Chen, H.-J. Ju, G.-X. Zhang and D.-Q. Zhang, Diketopyrrolopyrrole-based conjugated polymer entailing triethylene glycols as side chains with high thin-film charge mobility without post-treatments, *Adv. Sci.*, 2017, **4**, 1700048.

21 A. Gumyusenge, X. Zhao, Y. Zhao and J. Mei, Attaining melt processing of complementary semiconducting polymer blends at 130 °C via side-chain engineering, *ACS Appl. Mater. Interfaces*, 2018, **10**, 4904–4909.

22 S. A. Park, D. H. Kim, Y. Choi, D. H. Lee, T. Park, S. Cho and M. Kim, Molecular symmetry effect on the morphology and self-aggregation of semiconducting polymers, *Polym. Chem.*, 2023, **14**, 374–382.

23 T. Jia, Z. Li, L. Ying, J. Jia, B. Fan, W. Zhong, F. Pan, P. He, J. Chen, F. Huang and Y. Cao, Asymmetric alkyl side-chain engineering of naphthalene diimide-based n-type polymers for efficient all-polymer solar cells, *Macromol. Rapid Commun.*, 2018, **39**, e1700765.

24 J. Cao, H. Wang, S. Qu, J. Yu, L. Yang, Z. Zhang, F. Du and W. Tang, 2D side-chain engineered asymmetric acceptors enabling over 14% efficiency and 75% fill factor stable organic solar cells, *Adv. Funct. Mater.*, 2020, **30**, 2006141.

25 J. Lee, A.-R. Han, H. Yu, T. J. Shin, C. Yang and J. H. Oh, Boosting the ambipolar performance of solution-processable polymer semiconductors via hybrid side-chain engineering, *J. Am. Chem. Soc.*, 2013, **135**, 9540–9547.

26 Y. Wang, E. Zeglio, H. Liao, J. Xu, F. Liu, Z. Li, I. P. Maria, D. Mawad, A. Herland, I. McCulloch and W. Yue, Hybrid alkyl-ethylene glycol side chains enhance substrate adhesion and operational stability in accumulation mode organic electrochemical transistors, *Chem. Mater.*, 2019, **31**, 9797–9806.

27 B. Kan, X. Chen, K. Gao, M. Zhang, F. Lin, X. Peng, F. Liu and A. K.-Y. Jen, Asymmetrical side-chain engineering of small-molecule acceptors enable high-performance nonfullerene organic solar cells, *Nano Energy*, 2020, **67**, 104209.

28 X. Chen, Z. Zhang, Z. Ding, J. Liu and L. Wang, Diketopyrrolopyrrole-based conjugated polymers bearing branched oligo(ethylene glycol) side chains for photovoltaic devices, *Angew. Chem., Int. Ed.*, 2016, **55**, 10376–10380.

29 B. Meng, H. Song, X. Chen, Z. Xie, J. Liu and L. Wang, Replacing alkyl with oligo(ethylene glycol) as side chains of conjugated polymers for close π-π stacking, *Macromolecules*, 2015, **48**, 4357–4363.

30 D. Aoki and H. Ajiro, Design of polyurethane composed of only hard main chain with oligo(ethylene glycol) units as side chain simultaneously achieved high biocompatible and mechanical properties, *Macromolecules*, 2017, **50**, 6529–6538.

31 M. Moser, L. R. Savagian, A. Savva, M. Matta, J. F. Ponder, T. C. Hidalgo, D. Ohayon, R. Hallani, M. Reisjalali, A. Troisi, A. Wadsworth, J. R. Reynolds, S. Inal and I. McCulloch, Ethylene glycol-based side chain length engineering in polythiophenes and its impact on organic electrochemical transistor performance, *Chem. Mater.*, 2020, **32**, 6618–6628.

32 T. Lei, J.-H. Dou and J. Pei, Influence of alkyl chain branching positions on the hole mobilities of polymer thin-film transistors, *Adv. Mater.*, 2012, **24**, 6457–6461.

33 J. Mei, K. R. Graham, R. Stalder and J. R. Reynolds, Synthesis of isoindigo-based oligothiophenes for molecular bulk heterojunction solar cells, *Org. Lett.*, 2010, **12**, 660–663.

34 R. K. Roy, E. B. Gowd and S. Ramakrishnan, Periodically grafted amphiphilic copolymers: Nonionic analogues of ionenes, *Macromolecules*, 2012, **45**, 3063–3069.

35 J. Liang, X. Zheng, L. He, H. Huang and W. Bu, Remarkable luminescence enhancement of chloroplatinum(II) complexes of hexaethylene glycol methyl ether substituted 2,6-bis(benzimidazol-2′-yl)pyridine in water triggered by PF_6^-, *Dalton Trans.*, 2014, **43**, 13174–13177.

36 P.-J. Voorter, A. McKay, J. Dai, O. Paravagna, N. R. Cameron and T. Junkers, Solvent-independent molecular weight determination of polymers based on a truly universal calibration, *Angew. Chem., Int. Ed.*, 2021, **61**, e202114536.

37 S. Hayashi, Highly crystalline and efficient red-emissive π-conjugated polymer film: Tuning of macrostructure for light-emitting properties, *Mater. Adv.*, 2020, **1**, 632–638.

38 Z. Liu, H. A. Becerril, M. E. Roberts, Y. Nishi and Z. Bao, Experimental study and statistical analysis of solution-shearing processed organic transistors based on an asymmetric small-molecule semiconductor, *IEEE Trans. Electron Devices*, 2009, **56**, 176–185.

39 Y. Ito, A. A. Virkar, S. Mannsfeld, J. H. Oh, M. Toney, J. Locklin and Z. Bao, Crystalline ultrasmooth self-assembled monolayers of alkylsilanes for organic field-effect transistors, *J. Am. Chem. Soc.*, 2009, **131**, 9396–9404.

40 Y. Shi, J. Liu, Y. Hu, W. Hu and L. Jiang, Effect of contact resistance in organic field–effect transistors, *Nano Sel.*, 2021, **2**, 1661–1681.

41 T. Lei, Y. Cao, Y. Fan, C.-J. Liu, S.-C. Yuan and J. Pei, High-performance air-stable organic field-effect transistors: Isoindigo-based conjugated polymers, *J. Am. Chem. Soc.*, 2011, **133**, 6099–6101.

42 M. Hambsch, T. Erdmann, A. R. Chew, S. Bernstorff, A. Salleo, A. Kiriy, B. Voit and S. C. B. Mannsfeld, Increased charge carrier mobility and molecular packing of a solution sheared diketopyrrolopyrrole-based donor-acceptor copolymer by alkyl side chain modification, *J. Mater. Chem. C*, 2019, **7**, 3665–3674.

43 J. Rivnay, S. Inal, A. Salleo, R. M. Owens, M. Berggren and G. G. Malliaras, Organic electrochemical transistors, *Nat. Rev. Mater.*, 2018, **3**, 17086.

44 D. Khodagholy, J. Rivnay, M. Sessolo, M. Gurfinkel, P. Leleux, L. H. Jimison, E. Stavrinidou, T. Herve, S. Sanaur, R. M. Owens and G. G. Malliaras, High transconductance organic electrochemical transistors, *Nat. Commun.*, 2013, **4**, 2133.

45 D. A. Bernards and G. G. Malliaras, Steady-state and transient behavior of organic electrochemical transistors, *Adv. Funct. Mater.*, 2007, **17**, 3538–3544.

46 S. Inal, G. G. Malliaras and J. Rivnay, Benchmarking organic mixed conductors for transistors, *Nat. Commun.*, 2017, **8**, 1767.

47 Y. Dai, S. Dai, N. Li, Y. Li, M. Moser, J. Strzalka, A. Prominski, Y. Liu, Q. Zhang, S. Li, H. Hu, W. Liu, S. Chatterji, P. Cheng, B. Tian, I. McCulloch, J. Xu and S. Wang, Stretchable redox-active semiconducting polymers for high-performance organic electrochemical transistors, *Adv. Mater.*, 2022, **34**, 2201178.

48 P. R. Paudel, V. Kaphle, D. Dahal, R. K. R. Krishnan and B. Lüssem, Tuning the transconductance of organic electrochemical transistors, *Adv. Funct. Mater.*, 2021, **31**, 2004939.

© 2023 The Author(s). Published by the Royal Society of Chemistry

RSC Appl. Polym., 2023, **1**, 292–303 | **303**